Two Dimensional Crowding Effect on Protein Folding at Interfaces Observed by Chiral Vibrational Sum Frequency Generation Spectroscopy

Journal:	*Physical Chemistry Chemical Physics*
Manuscript ID	CP-COM-10-2017-007061.R3
Article Type:	Communication
Date Submitted by the Author:	17-Aug-2018

Complete List of Authors:	Liu, Wei; Yale University, Chemistry Fu, Li; PNNL Wang, Zhuguang; Yale Univsersity, Chemistry Sohrabpour, Zahra; University of Minnesota, Chemistry Li, Xiaobai; Yale University, Chemistry Liu, Yuting; Yale University, Chemistry Wang, Hongfei; Pacific Northwest National Laboratory, Molecular Sciences Laboratory Yan, Elsa; Yale, Chemistry

SCHOLARONE™
Manuscripts

Two Dimensional Crowding Effect on Protein Folding at Interfaces Observed by Chiral Vibrational Sum Frequency Generation Spectroscopy

Wei Liu[†], Li Fu[†,§], Zhuguang Wang[†], Zahra Sohrabpour[†], Xiaobai Li[†], Yuting Liu[†], Hong-fei Wang[#], and Elsa C. Y. Yan[†]*

†Department of Chemistry, Yale University, 225 Prospect Street, New Haven, Connecticut 06520, United States

§Current Address: Sanofi-Genzyme, Framingham, MA, 01701, United States

#Department of Chemistry, Fudan University, 220 Handan Road, Yangpu District, Shanghai 200433, China

*To whom correspondence should be addressed. E-mail: elsa.yan@yale.edu

ABSTRACT: Crowding effect is prevalent in cellular environment due to high concentration of biomacromolecules. It can alter structures and dynamics of proteins and thus impact protein functions. Crowding effect is important not only in 3-dimensional cytoplasm but also 2-dimensional (2D) cell surface due to presence of membrane proteins and glycosylation of membrane proteins and phospholipids. These proteins and phospholipids – with limited translational degree of freedom along the surface normal – are confined in 2D space. Although crowding effect at interfaces has been studied by adding crowding agents to bulk solution, 2D crowding effect remains largely unexplored. This is mostly due to challenges in controlling 2D crowding and synergetic use of physical methods for in situ protein characterization. To address these challenges, we applied chiral vibrational sum frequency generation (SFG) spectroscopy to probe sp1 zinc finger (ZnF), a 31-amino acid protein, folding into the β-hairpin/α-helix ($\beta\beta\alpha$) motif upon binding to Zn^{2+}. We anchored ZnF at the air/water interface via covalent linkage of ZnF to palmitic acid and controlled 2D crowding by introducing neutral lipid as a spacer. We obtained chiral amide I SFG spectra upon addition of Zn^{2+} and/or spacer lipid. The chiral SFG spectra show that interfacial crowding in the absence of spacer lipid hinders ZnF from folding into the $\beta\beta\alpha$ structure even in the presence of Zn^{2+}. The results establish a paradigm for future quantitative, systematic studies of interfacial crowding effects.

Macromolecular crowding is crucial to cell functions.[1-3] The concentration of macromolecules can be as high as 200-300 g/L in cytoplasm, making cytosolic proteins reside and function in a crowded environment. This macromolecular crowding can change protein structures and dynamics. Thus, neglecting molecular crowding can jeopardize biological relevance of *in vitro* studies conducted in diluted aqueous solution.[4-8] Similar to cytoplasm in 3-dimensional space, cell surface in 2-dimensional (2D) space is also highly crowded with macromolecules. While phospholipids construct the basic structures of cell membrane, the protein content of cell membranes can be as high as 1:1 protein:lipid by weight. These proteins occupy cell surface area from 30 to 80%.[1, 9, 10] These proteins include scaffold proteins that form signaling complexes on cell surfaces and, peripheral proteins physically adsorbed on membrane surface. Conventional consideration of crowding effect of call membrane focuses on the crowded environment of the lipid membrane region, which in principle constitutes a 3D space including not only 2D cell surface but also an additional dimension of membrane thickness. Here, we consider the crowding effect at the hypothetically thin interface between the lipid head groups and aqueous phase. This unconventional and novel consideration of 2D-crowding effect is important because transmembrane proteins can have extracellular domain that can be as large as 100 kDa and both membrane proteins and phospholipids can be glycosylated with hydrophilic oligosaccharides.[11, 12] Hence, cell surface is not merely the interface between phospholipid head groups and aqueous phase but with abundant macromolecules. This crowding environment can change protein structures, dynamics, and orientation at cell surface, and thereby govern protein functions.[13-16] Recent evidence suggests that cells make use of 2D crowding to direct cellular functions, e.g., modulating curvature to control cell migration.[17, 18] Hence, establishing a feasible platform for probing 2D interfacial crowding will introduce opportunities for quantitative, systematic studies of interfacial crowding in 2D space, and thus will have implications in molecular understanding of various cellular functions.

Crowding effect on protein folding at interfaces has been reported. Grobner and coworkers studied amyloid proteins on membrane surfaces.[19, 20] Using a combination of circular dichorism and infrared reflection-absorption spectroscopy, they examined misfolding of the proteins at high concentration (~10^2 g/L) of crowding agents (i.e., inert synthetic polymers) in bulk aqueous solutions and found that the crowding agents impacted the misfolding behaviors at interfaces. While these pioneering studies have demonstrated molecular crowding effect on protein folding at interfaces, the crowding agents undergo 3D translational diffusion in bulk solution. Interfacial molecular crowding confined in 2D space has remained largely unexplored. This is mostly due to challenges in controlling 2D crowding environment and synergetic use of surface-specific methods for in situ protein characterization.

To overcome the challenges, we designed an experiment (Fig. 1) to probe 2D crowding effect. The overall design involved a lipid-protein construct and application of chiral vibrational sum frequency generation spectroscopy (SFG) to probe protein structures at the air/water interfaces.[21-23] The lipid-protein construct contains a model protein, zinc finger, linked to a palmitic acid and thus can be anchored at the air/water interface (Fig. 1A). Folding of zinc finger can be induced by adding Zn^{2+} while 2D crowding can be controlled by adding lipid as spacer at the interface. Chiral SFG, which is effective in distinguishing protein secondary structures at interfaces, can be used to monitor the folding of zinc finger at the air/water interface.[24, 25] Hence, the experimental design allows for observing crowding effect on zinc finger folding at the interface.

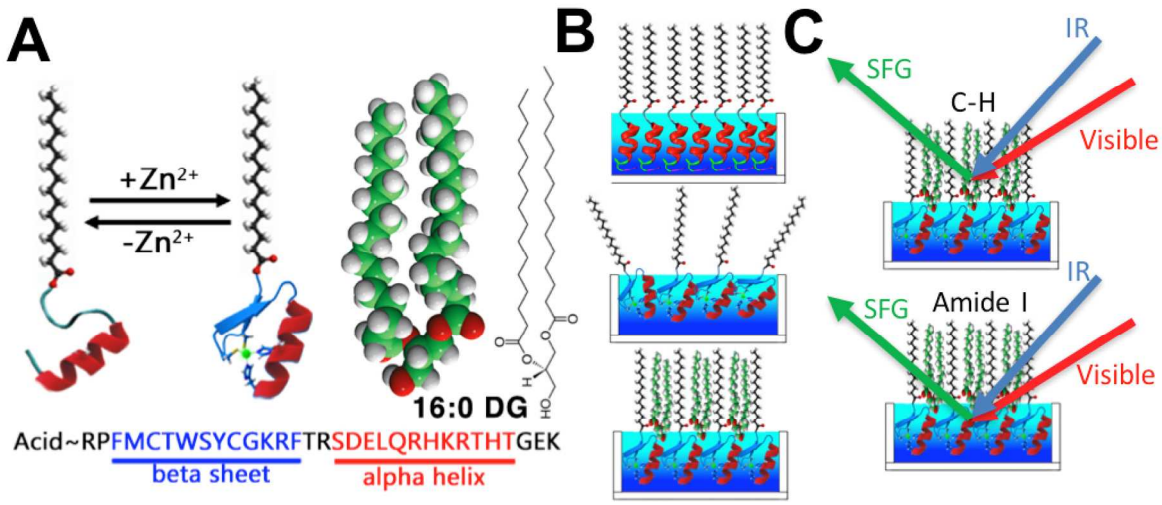

Figure 1. Experimental Design. (A) Zinc finger covalently linked to palmitic acid for surface anchoring; zinc ion induces folding of the N-terminal domain (blue) from disordered structure to β-sheet; 1,2-dipalmitoyl-sn-glycerol (DG) is used as spacer to control the 2D crowding at the air/water interface. (B) Three conditions for probing zinc finger folding at the air/water interface: (i) in the absence of both Zn^{2+} and the DG spacer lipid; (ii) in the presence of Zn^{2+} and absence of DG, (iii) in the presnce of both Zn^{2+} and DG. (C) Acqusition of vibrational SFG spectra of surface-anchored zinc finger in the C-H stretch region to probe structures of the alkyl chains of the palmityl group and DG, and in the amide I region to probe protein structure of zinc finger.

We used chiral vibrational SFG to observe ZnF folding at the air/water interface. Chiral SFG[5, 21, 22, 26] is a special case of vibrational SFG spectroscopy.[27-29] Chiral SFG is performed using selected polarizations of the incident beams and SFG output for measurements of orthogonal second-order susceptibility elements ($\chi^{(2)}_{i\neq j\neq k}$, where *i, j, k* = x, y, or z that are laboratory coordinates).[5, 21, 22, 26, 30] Chen's group reported the first chiral amide I vibrational spectrum of proteins[23] while Geiger's group reported chiral C-H stretch signals from DNA at interfaces.[31] Petersen and coworkers recently showed that chiral SFG could be used to detect water molecules in chiral supramolecular structures oriented by the DNA molecules.[32] Wang's

group demonstrated novel polarization dependent techniques to measure interfering chiral and achiral contributions to surface nonlinear signals[33] and studied the chiral and prochiral vibrational signatures.[34] Chiral SFG has also been combined with advanced optical techniques, such as heterodyne detection[35] and ultrafast pump-probe techniques.[36] Relevant to the current study of 2D crowding effect is our previous work. We showed that chiral SFG provides characteristic peptide amide I and N-H stretch vibrational signatures for distinguishing protein secondary structures at interfaces.[24, 25, 37-39] In particular, the chiral SFG signatures of α-helices include prominent N-H stretch but muted amide I signals while the chiral SFG signatures of β-sheets include both N-H stretch and amide I chiral SFG signals. These signatures have been increasingly used for protein characterization at interfaces.[36, 40-42] They are background-free from water solvent and other achiral interfacial molecules. More importantly, the chiral amide I signatures are active for β-sheet but silent for α-helix, thus allowing straightforward spectral interpretation.[24, 25, 37-39] In this study, we leveraged these advantages of chiral SFG to study 2D crowding effect on protein folding at interfaces.

In this study, we chose sp1 zinc finger (ZnF) as a model system. Containing 31 amino acids, it is ubiquitous in DNA- or RNA-binding proteins.[43] Without Zn^{2+}, the N-terminal domain is unfolded in disordered structures while the C-terminal domain is dynamic with a tendency to form a short α-helical segment (Fig. 1A).[44] As shown by the NMR structure of ZnF (PDB 1VA2),[44] upon binding to Zn^{2+}, the N-terminal domain (blue, Scheme 1) folds into a β-hairpin (two antiparallel β-strands and one β-turn) while the C-terminal α-helix is stabilized. The β-hairpin contributes two cysteine residues and the α-helix contributes two histidine residues to coordinate a Zn^{2+} ion, resulting in a $\beta\beta\alpha$-motif (Scheme 1). Because the folded and unfolded structures of ZnF are known[44] and ZnF folding can be triggered by addition of Zn^{2+}, we used ZnF as a model system for examining interfacial crowding effect.

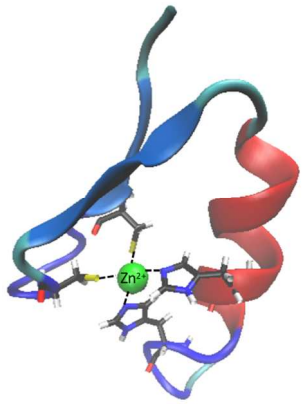

Scheme 1. The $\beta\beta\alpha$-motif of the sp1 zinc finger (ZnF) with coordination of Zn^{2+} to two cysteine residues and two histidine residues.

Here, we provide details in setting up the molecular systems for probing interfacial crowding effect. We attached sp1 zinc finger (ZnF) to palmitic acid via an amide linkage. The palmityl-ZnF construct is amphiphilic, thus situating at the air/water interface. The first two amino acids of ZnF at the N-terminus are hydrophilic and not part of the β-hairpin structure. These two amino acids, together with an additional amide group in the covalent linkage, can provide not only flexibility allowing for β-hairpin formation (as illustrated in chiral SFG results discussed later) but also situate the ZnF protein into the aqueous phase. With this amphiphilic construct, ZnF is not likely to expose to the air phase as reported by Weidner's recent work on the GALA peptide that has a cell-penetrating function with periodic clusters of hydrophobic residues along the 30-amino acid sequence.[45, 46] A neutral lipid, 1,2-dipalmitoyl-sn-glycerol (DG) was used as the spacer (Fig. 1). Addition of the spacer DG lipid can modulate macromolecular crowding caused by tightly packed palmityl-ZnF at the air/water interface. The cross section areas of the molecules are roughly estimated to be palmitic acid (~ 10 $Å^2$), DG (~ 50 $Å^2$), and folded palmityl-ZnF (~300 $Å^2$) (see the SI). In response to addition of DG, we used chiral SFG to examine whether Zn^{2+} can induce folding of palmityl-ZnF at the air/water interface. Chiral SFG is inactive in the amide I region for α-helical and disordered structures but active for

β-sheets.[24, 25, 37-39] Hence, unfolded palmityl-ZnF will not provide any chiral amide I signal and only folded palmityl-ZnF in the $\beta\beta\alpha$ structure will give chiral amide I signals. Therefore, chiral SFG allowed for straightforward detection of ZnF folding.

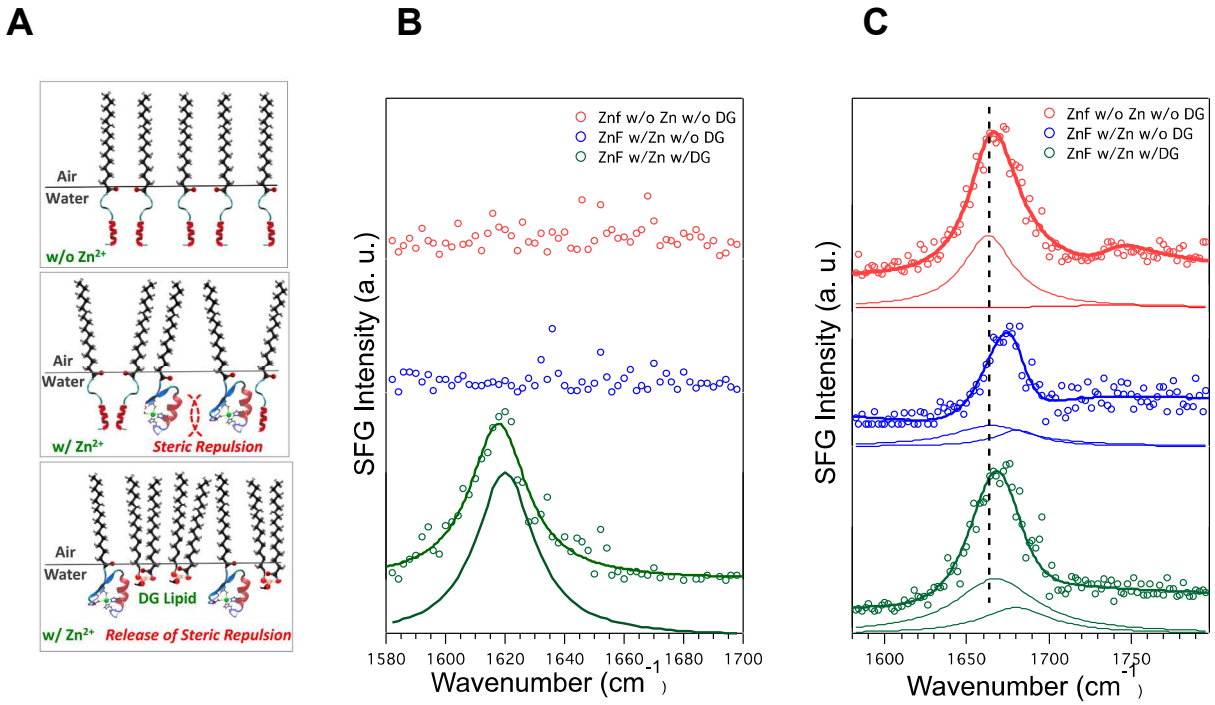

Figure 2. Chiral and achiral SFG spectra of palmityl-ZnF at the air/water interface in the amide I regions. (A) Three conditions for obtaining the spectra from top to bottom: (1) without Zn^{2+} and without DG, (2) with Zn^{2+} and without DG, and (3) with Zn^{2+} and with DG. (B) Chiral and (C) achiral amide I spectra of palmityl-ZnF at the air/water interface under the three conditions. (Buffer: 10 mM phosphate, pH 7.4, concentration of palmityl-ZnF = 5 μM, concentration of Zn^{2+} = 2 mM, and DG:palmityl-ZnF = 5:1)

We performed the SFG spectroscopic studies of palmityl-ZnF at the air/water interface under three major conditions (Fig. 2A): (1) in the absence of both Zn^{2+} and DG spacer, (2) in the presence of Zn^{2+} and absence of DG spacer and (3) in the presence of both Zn^{2+} and DG spacer at a ratio of 5:1 DG:palmityl-ZnF (Fig. 2). Based on the adsorption free energies of DG and palmityl-ZnF at the air/water interface (see the SI), the ratio of DG: palmityl-ZnF was estimated to be ~ 6:1 at the interface under the assumption that the interaction free energy between lipid

and palmityl-ZnF is the same as that between lipids and that between the palmityl-ZnF molecules. The ratio of 6:1 is a reasonable estimate because DG contains two carbon chains and a relatively small head group and thus should have higher tendency to adsorb onto the air/water interface, whereas palmityl-ZnF has only one carbon chain and should have lower tendency to adsorb onto the interface. Therefore, the DG lipid should be slightly enriched at the interface, i.e., the DG:palmityl-ZnF ratio from 5:1 to 6:1. This estimate suggests that DG can introduce enough space for the surface anchored ZnF to fold in contrast to the conditions of without DG lipid. In performing the experiments, we used the same samples for the conditions of with and without Zn^{2+} by carefully injecting $ZnCl_2$ stock solution to a final concentration of 2 mM using a micro-syringe and then obtained a spectrum.

Using a scanning SFG spectrometer[47] (EKSPLA, see the SI), we obtained not only chiral amide I spectra (Fig. 2B), but also achiral amide I spectra (Fig. 2C) and C-H stretch spectra (Fig. 3). The amide I spectra (Fig. 2) provide structural information about ZnF; the C-H stretch spectra (Fig. 3) provide structural information about alkyl chains of the palmityl group of palmityl-ZnF and the DG lipid at the air/water interface. We prepared all samples in a circular Teflon beaker (diameter of 4 cm) consisting of 5.0 ml of aqueous solution (10 mM phosphate, pH 7.4) with palmityl-ZnF (5 μM). Aside from the above three conditions (Fig. 2A), we also obtained the amide I spectra in the absence of Zn^{2+} and presence of DG spacer, yielding results that are similar to the spectra obtained under the first condition (absence of both Zn^{2+} and DG) and thus only presented in the SI.

We took the chiral SFG spectra (Fig. 2B) using the polarization setting of *psp* (*p*-polarized SFG, *s*-polarized visible, and *p*-polarized IR). In the absence of both Zn^{2+} and DG, the spectrum (red) is silent. In the presence of Zn^{2+} and absence of DG, the spectrum (blue) is also silent. Only in the presence of both Zn^{2+} and DG does the chiral spectrum (green) show a prominent amide I signal. These results can be interpreted using a simple molecular picture. Under the first condition (w/o Zn^{2+} and w/o DG, red), ZnF is in the unfolded state due to the absence of Zn^{2+}.

Thus, it contains a disordered N-terminal domain and a short α-helical segment. The absence of β-sheet structure leads to a silent chiral amide I spectrum. Under the second condition (w/ Zn^{2+} and w/o DG, blue, Fig. 2B), palmityl-ZnF (5 μM) is saturated at the air/water interface (see absorption isotherm in the SI). The tightly packed molecular environment does not allow ZnF to fully fold into the $\beta\beta\alpha$ structure. Hence, the β-sheet content is low and chiral amide I signal cannot be detected. Under the third condition (w/ Zn^{2+} and w/ DG, green, Fig. 2B), addition of DG (DG:palmityl-ZnF = 5:1) spaces out ZnF at the air/water interface and releases the steric constraint. Hence, ZnF has enough room to fold into the $\beta\beta\alpha$ structure at the interface. The two β-strands in the structure can then contribute to the chiral amide I signal. The observed amide I band is fitted to a Lorentzian line shape (see the SI for the equation),centered at 1620.1 ± 1.4 cm^{-1}. Indeed, an amide I band at ~1620 cm^{-1} is characteristic of the B1 amide I vibrational mode of antiparallel β-sheets.[48, 49]

We also obtained achiral SFG amide I spectra (Fig. 2C) using the polarization setting of *ssp* (*s*-polarized SFG, *s*-polarized visible, and *p*-polarized IR). The spectra were obtained under the same three conditions (Fig. 2A). All three spectra show a major peak (Fig. 2C) with some variations in position, width, and intensity. In general, deconvolution of amide I vibrational spectra is challenging due to overlapping of contributions from various protein secondary structures. Here, we aim to provide the simplest interpretation, which is guided by (1) the results of chiral SFG spectra (Fig. 2B) and (2) previously reported assignments of amide I bands to secondary structures.[48-50] The first (red) spectrum (Fig. 2C, w/o Zn^{2+} and w/o DG) shows a relatively high intensity. The 1740-cm^{-1} band is assigned to carbonyl (C=O) stretch vibrational band possibly due to the palmityl group and protonated carboxylic acid residues. In the absence of both Zn^{2+} and DG, palmityl-ZnF is unfolded and tightly packed at the air/water interface, thus allowing for detection of this carbonyl peak. The major peak is an amide I band centered at 1664 ± 0.9 cm^{-1} is assigned to disordered and/or α-helical structures. The 1664 cm^{-1} band is at the high end of standard amide I frequency for α-helices.[48, 49] However, assignment of amide I bands at

~1665 cm^{-1} to α-helices is not uncommon, especially for short and distorted α-helices.[50-53] In Fig. 2C, the second (blue) achiral spectrum (w/ Zn^{2+} and w/o DG) shows a decrease in SFG intensity (~25% of the first spectrum, see fitting results in the SI) and a narrower peak width. This narrow peak can be fitted into one amide I band centered at 1664.7 ± 1.0 cm^{-1}, assigned to disordered and/or α-helical structures with possible contribution from β-turn.[48, 49] The presence of Zn^{2+} triggers the propensity of ZnF folding. However, the steric repulsion among the tightly packed palmityl-ZnF in the 2D environment likely destabilizes and/or disorders the $\beta\beta\alpha$-fold, leading to a decrease in the SFG intensity. Relative to the second spectrum, the third (green, Fig. 2C) achiral spectrum (w/ Zn^{2+} and w/ DG) shows higher intensity (~75% of the first spectrum) and wider peak width (see fitting results in the SI). The peak (green) can be fitted into a single vibrational band centered at 1655.2 ± 1.0 cm^{-1} (see the SI). Although using two vibrational bands can improve the fitting, we cannot identify a unique set of parameters to define the two peaks. Guided by the chiral SFG results (Fig. 2B), we fitted the spectrum into two bands (see the SI). We assigned the 1667-cm^{-1} band to α-helix with possible contributions from disordered structures and β-turn, and the 1682-cm^{-1} band to β-sheet.

Under the same three conditions (Fig. 2A), we also obtained (achiral) C-H stretch spectra to examine the structures of alkyl chains in the palmityl group and DG lipid. It has been established that (achiral) SFG spectra in the C-H stretch spectra can reveal structures and orientations of alkyl chains at interfaces.[54-56] Figure 3 presents the *ssp* and *ppp* spectra (see the fitting results in the SI). In the *ssp* spectra, the peaks at 2850 cm^{-1} and 2870 cm^{-1} were assigned to CH_2 symmetric stretch (CH_2 SS) and CH_3 symmetric stretch (CH_3 SS), respectively. The broad peak at around 2920 cm^{-1} to 2980 cm^{-1} is a combination of CH_2 Fermi resonance (CH_2 FR), CH_3 Fermi resonance (CH_3 FR), and CH_3 asymmetric stretch (CH_3 AS).[54] Under the first condition (red, without Zn^{2+} and without DG), the CH_3 SS is very strong compared to CH_2 SS, which is characteristic of well-orientated carbon chains at the interface. It is well known that the highly ordered alkyl chains result in the methyl groups pointing at vertical direction to yield maximum

symmetric stretch signal in the *ssp* spectrum while the CH_2 symmetric stretch dipoles pointing up and down alternatively lead to cancelation. Under the second condition (blue, with of Zn^{2+} and without DG), the CH_3 SS is significantly reduced while the CH_2 SS is enhanced, indicating a disruption of the alignment of the alkyl chains. Addition of Zn^{2+} triggers the tendency of ZnF folding; however, the 2D crowding environment leads to steric repulsion among ZnF and disorients the alkyl chains. Under the third condition (green, with Zn^{2+} and with DG), the CH_3 SS is significantly enhanced while the CH_2 SS almost vanishes. This suggests that the DG spacer releases the steric hindrance and the alkyl chains from both DG and the palmityl group interact to form an ordered and compact film. In the *ppp* spectra, only the CH_3 AS is predominant. The decrease in the intensity of CH_3 AS in the presence of Zn^{2+} but absence of DG (blue), as well as the increases in the intensity of CH_3 AS in the presence of both Zn^{2+} and DG (green) support the conclusion drawn from the *ssp* C-H stretch spectra that the folded ZnF cause the carbon chains to disorient and the DG lipid spacer releases molecular crowding and enable the carbon chains to regain the alignment and packing, supporting the interpretation of the amide I spectra (Fig. 2).

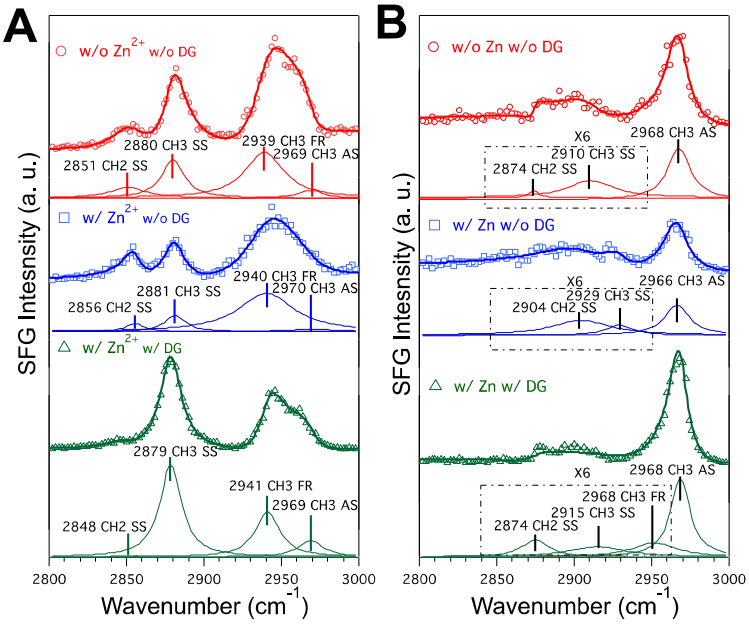

Figure 3. SFG spectra of palmityl-ZnF at the air/water interface in the C-H stretch region. (A) Spectra obtained using the *ssp* polarization setting and (B) spectra obtained using the *ppp*

polarization setting. Three conditions from top to bottom: (red) without Zn^{2+} and without DG, (blue) with Zn^{2+} and without DG, and (green) with Zn^{2+} and with DG.

In summary, the above SFG studies support the observation of the crowding effect on protein folding at interfaces. In the presence of DG spacer, addition of Zn^{2+} induces folding of ZnF into the $\beta\beta\alpha$ structure. However, in the absence of DG spacer, additional of Zn^{2+} cannot induce folding of ZnF into the $\beta\beta\alpha$ structure due to crowding interfacial environments. In this crowding environment, the tendency of ZnF folding in the presence of Zn^{2+} disorients the alkyl chains of the palmityl group and DG lipid at the interface. Addition of DG lipid spacer releases the interfacial crowding such that the alkyl chains can resume the ordered packing at the interface while ZnF can fold into the $\beta\beta\alpha$ structure.

In this study, we obtained both chiral and conventional (achiral) SFG spectra in parallel. The results allow for a direct comparison of the chiral and achiral SFG methods for protein characterization at interfaces. This comparison has demonstrated the advantage of chiral SFG particularly for studying proteins that contain multiple secondary structures. The selectivity of chiral SFG to the amide I modes of β-sheets enables detection of β-sheets without spectral interference from helical and disordered protein structures. This unique selectivity to β-sheets overcomes a major challenge of using vibrational methods (not only for achiral SFG but also general infrared spectroscopy) for studying amide I modes of protein structures due to spectral overlapping of amide I bands for various protein secondary structures.[24, 25, 37-39] The distinct selectivity of chiral SFG to proteins in β-sheet structures has mostly eliminated the need of spectral deconvolution and thus greatly simplified spectral interpretation.

To conclude, the above experimental studies of surface-anchored proteins using chiral SFG provides a new approach for investigating 2D crowding effect on proteins at interfaces. This approach can be modified to enable systematic studies of 2D crowding, e.g., impacts of surface population, surface roughness, surface viscosity, and electrolyte concentration. The approach can also be combined with advanced optical techniques, e.g., heterodyne detection,[57, 58] pump-probe

ultrafast studies,[36, 59] and multi-dimensional spectroscopy.[60, 61] Implementation of these techniques will expand the approach to address a wide range of problems related to interfacial crowding, such as ultrafast dynamics and site-specific protein interactions. These studies will advance our fundamental understanding of 2D crowding effect at interfaces with implications in revealing molecular mechanism of life processes on cell membrane surfaces.

Conflicts of interest.

There are no conflicts of interest to declare.

Supporting Information.

SFG setup, materials, experimental methods, cross-section of molecular systems, spectral fitting parameters and adsorption isotherms of palmityl-ZnF and DG at the air/water interface.

Acknowledgment.

This work was partially supported by NSF Grant CHE 1213362 to EY. Part of this work was conducted at the William R. Wiley Environmental Molecular Sciences Laboratory (EMSL), a national scientific user facility located at the Pacific Northwest National Laboratory and sponsored by the Department of Energy's Office of Biological and Environmental Research (BER). LF was a William Wiley Postdoc at the EMSL, and HFW was a chief scientist at the Physical and Computational Sciences Directorate (PCSD) at PNNL during the SFG measurements in this work.

Reference:

1. R. J. Ellis, *Trends in biochemical sciences*, 2001, **26**, 597-604.
2. H.-X. Zhou, G. Rivas and A. P. Minton, *Annual Review of Biophysics*, 2008, **37**, 375-397.
3. J. A. Dix and A. S. Verkman, *Annual Review of Biophysics*, 2008, **37**, 247-263.
4. B. van den Berg, R. Wain, C. M. Dobson and R. J. Ellis, *The EMBO Journal*, 2000, **19**, 3870-3875.
5. J. M. Perry, A. J. Moad, N. J. Begue, R. D. Wampler and G. J. Simpson, *Journal of Physical Chemistry B*, 2005, **109**, 20009-20026.
6. N. Tokuriki, M. Kinjo, S. Negi, M. Hoshino, Y. Goto, I. Urabe and T. Yomo, *Protein Sci.*, 2004, **13**, 125-133.
7. X. Ai, Z. Zhou, Y. Bai and W.-Y. Choy, *J. Am. Chem. Soc.*, 2006, **128**, 3916-3917.
8. S. Mukherjee, M. M. Waegele, P. Chowdhury, L. Guo and F. Gai, *J. Mol. Biol.*, 2009, **393**, 227-236.
9. P. F. Devaux and M. Seigneuret, *Biochimica et Biophysica Acta (BBA)-Reviews on Biomembranes*, 1985, **822**, 63-125.
10. H. Kirchhoff, S. Haferkamp, J. F. Allen, D. B. Epstein and C. W. Mullineaux, *Plant physiology*, 2008, **146**, 1571-1578.
11. C. R. H. Raetz, C. M. Reynolds, M. S. Trent and R. E. Bishop, *Annual Review of Biochemistry*, 2007, **76**, 295-329.
12. J. Kopitz, *Histochemistry and Cell Biology*, 2017, **147**, 175-198.
13. B. Alberts, A. Johnson, P. Walter, J. Lewis, M. Raff and K. Roberts, *New York and London: Garland Science*, 2008, **4**.
14. M. Edidin, *Nature Rev. Mol. Cell Biol.*, 2003, **4**, 414-418.
15. J. Derganc and A. Čopič, *Biochimica et Biophysica Acta (BBA)-Biomembranes*, 2016, **1858**, 1152-1159.
16. H.-X. Zhou, *The journal of physical chemistry B*, 2009, **113**, 7995-8005.
17. J. C. Stachowiak, C. C. Hayden and D. Y. Sasaki, *Proceedings of the National Academy of Sciences*, 2010, **107**, 7781-7786.
18. J. C. Stachowiak, E. M. Schmid, C. J. Ryan, H. S. Ann, D. Y. Sasaki, M. B. Sherman, P. L. Geissler, D. A. Fletcher and C. C. Hayden, *Nature cell biology*, 2012, **14**, 944-949.
19. C. Aisenbrey, B. Bechinger and G. Gröbner, *Journal of molecular biology*, 2008, **375**, 376-385.
20. M. Bokvist and G. Gröbner, *Journal of the American Chemical Society*, 2007, **129**, 14848-14849.
21. E. C. Yan, L. Fu, Z. Wang and W. Liu, *Chemical reviews*, 2014, **114**, 8471-8498.
22. L. M. Haupert and G. J. Simpson, *Annual Review of Physical Chemistry*, 2009, **60**, 345-365.
23. J. Wang, X. Y. Chen, M. L. Clarke and Z. Chen, *Proc Natl Acad Sci U S A*, 2005, **102**, 4978-4983.

24. L. Fu, J. Liu and E. C. Y. Yan, *Journal of the American Chemical Society*, 2011, **133**, 8094-8097.
25. L. Fu, Z. Wang and E. C. Y. Yan, *International journal of molecular sciences*, 2011, **12**, 9404-9425.
26. H.-F. Wang, W. Gan, R. Lu, Y. Rao and B.-H. Wu, *International Reviews in Physical Chemistry*, 2005, **24**, 191-256.
27. G. Richmond, *Chemical reviews*, 2002, **102**, 2693-2724.
28. Y. Shen, *Nature*, 1989, **337**, 519-525.
29. K. Eisenthal, *Chemical reviews*, 1996, **96**, 1343-1360.
30. A. J. Moad and G. J. Simpson, *The Journal of Physical Chemistry B*, 2004, **108**, 3548-3562.
31. G. Y. Stokes, J. M. Gibbs-Davis, F. C. Boman, B. R. Stepp, A. G. Condie, S. T. Nguyen and F. M. Geiger, *Journal of the American Chemical Society*, 2007, **129**, 7492-7493.
32. M. L. McDermott, H. Vanselous, S. A. Corcelli and P. B. Petersen, *ACS Central Science*, 2017, **3**, 708-714.
33. Y.-y. Xu, Y. Rao, D.-s. Zheng, Y. Guo, M.-h. Liu and H.-f. Wang, *The Journal of Physical Chemistry C*, 2009, **113**, 4088-4098.
34. L. Fu, Y. Zhang, Z.-H. Wei and H.-F. Wang, *Chirality*, 2014, **26**, 509-520.
35. M. Okuno and T.-a. Ishibashi, *The Journal of Physical Chemistry Letters*, 2014, **5**, 2874-2878.
36. J. Tan, B. Zhang, Y. Luo and S. Ye, *Angewandte Chemie International Edition*, 2017, **56**, 12977-12981.
37. L. Fu, Z. Wang and E. C. Y. Yan, *Chirality*, 2014, **26**, 521-524.
38. Z. Wang, L. Fu, G. Ma and E. C. Yan, *Langmuir*, 2015, **31**, 11384-11398.
39. E. C. Yan, Z. Wang and L. Fu, *The Journal of Physical Chemistry B*, 2015, **119**, 2769-2785.
40. K. Meister, A. Bäumer, G. R. Szilvay, A. Paananen and H. J. Bakker, *The Journal of Physical Chemistry Letters*, 2016, **7**, 4067-4071.
41. K. Meister, A. Paananen and H. J. Bakker, *Physical Chemistry Chemical Physics*, 2017, **19**, 10804-10807.
42. M. Okuno and T.-a. Ishibashi, *The Journal of Physical Chemistry C*, 2015, **119**, 9947-9954.
43. A. Klug and D. Rhodes, *Trends in Biochemical Sciences*, 1987, **12**, 464-469.
44. S. Oka, Y. Shiraishi, T. Yoshida, T. Ohkubo, Y. Sugiura and Y. Kobayashi, *Biochemistry*, 2004, **43**, 16027-16035.
45. D. Schach, C. Globisch, S. J. Roeters, S. Woutersen, A. Fuchs, C. K. Weiss, E. H. G. Backus, K. Landfester, M. Bonn, C. Peter and T. Weidner, *The Journal of Chemical Physics*, 2014, **141**, 22D517.
46. D. K. Schach, W. Rock, J. Franz, M. Bonn, S. H. Parekh and T. Weidner, *Journal of the*

American Chemical Society, 2015, **137**, 12199-12202.
47. Z. Lu, A. Karakoti, L. Velarde, W. Wang, P. Yang, S. Thevuthasan and H.-f. Wang, *The Journal of Physical Chemistry C*, 2013, **117**, 24329-24338.
48. L. K. Tamm and S. A. Tatulian, *Quarterly Reviews of Biophysics*, 1997, **30**, 365-429.
49. A. Barth and C. Zscherp, *Quarterly Reviews of Biophysics*, 2003, **35**, 369-430.
50. M. D. Bazzi and R. W. Woody, *Biophysical Journal*, 1985, **48**, 957-966.
51. K. Das, *Colloids and Surfaces A: Physicochemical and Engineering Aspects*, 2015, **v. 468**, pp. 56-61-2015 v.2468.
52. U. Görne-Tschelnokow, A. Strecker, C. Kaduk, D. Naumann and F. Hucho, *The EMBO Journal*, 1994, **13**, 338-341.
53. K. J. Rothschild and N. A. Clark, *Biophysical Journal*, 1979, **25**, 473-487.
54. R. Lu, W. Gan, B.-h. Wu, Z. Zhang, Y. Guo and H.-f. Wang, *The Journal of Physical Chemistry B*, 2005, **109**, 14118-14129.
55. J. C. Conboy, M. C. Messmer and G. L. Richmond, *The Journal of Physical Chemistry*, 1996, **100**, 7617-7622.
56. G. Ma and H. C. Allen, *Langmuir*, 2006, **22**, 5341-5349.
57. I. V. Stiopkin, H. D. Jayathilake, A. N. Bordenyuk and A. V. Benderskii, *Journal of the American Chemical Society*, 2008, **130**, 2271-2275.
58. S. Yamaguchi and T. Tahara, *The Journal of Chemical Physics*, 2008, **129**, 101102.
59. M. A. Donovan, Y. Y. Yimer, J. Pfaendtner, E. H. G. Backus, M. Bonn and T. Weidner, *Journal of the American Chemical Society*, 2016, **138**, 5226-5229.
60. Z. Ganim, H. S. Chung, A. W. Smith, L. P. DeFlores, K. C. Jones and A. Tokmakoff, *Accounts of Chemical Research*, 2008, **41**, 432-441.
61. W. Xiong, J. E. Laaser, R. D. Mehlenbacher and M. T. Zanni, *Proceedings of the National Academy of Sciences*, 2011, **108**, 20902-20907.